Atmos. Chem. Phys., 15, 6305–6322, 2015
www.atmos-chem-phys.net/15/6305/2015/
doi:10.5194/acp-15-6305-2015

Atmospheric Chemistry and Physics
Open Access

Connecting the solubility and CCN activation of complex organic aerosols: a theoretical study using solubility distributions

I. Riipinen[1,2], **N. Rastak**[1], **and S. N. Pandis**[2,3]

[1]Department of Environmental Science and Analytical Chemistry, Stockholm University, Stockholm, Sweden
[2]Center of Atmospheric Particle Studies, Carnegie Mellon University, Pittsburgh, PA, USA
[3]Department of Chemical Engineering, University of Patras, Patras, Greece

Correspondence to: I. Riipinen (ilona.riipinen@aces.su.se)

Received: 26 October 2014 – Published in Atmos. Chem. Phys. Discuss.: 17 November 2014
Revised: 15 April 2015 – Accepted: 11 May 2015 – Published: 10 June 2015

Abstract. We present a theoretical study investigating the cloud activation of multicomponent organic particles. We modeled these complex mixtures using solubility distributions (analogous to volatility distributions in the VBS, i.e., volatility basis set, approach), describing the mixture as a set of surrogate compounds with varying water solubilities in a given range. We conducted Köhler theory calculations for 144 different mixtures with varying solubility range, number of components, assumption about the organic mixture thermodynamics and the shape of the solubility distribution, yielding approximately 6000 unique cloud condensation nucleus (CCN)-activation points. The results from these comprehensive calculations were compared to three simplifying assumptions about organic aerosol solubility: (1) complete dissolution at the point of activation; (2) combining the aerosol solubility with the molar mass and density into a single effective hygroscopicity parameter κ; and (3) assuming a fixed water-soluble fraction $\varepsilon_{\mathrm{eff}}$. The complete dissolution was able to reproduce the activation points with a reasonable accuracy only when the majority (70–80 %) of the material was dissolved at the point of activation. The single-parameter representations of complex mixture solubility were confirmed to be powerful semi-empirical tools for representing the CCN activation of organic aerosol, predicting the activation diameter within 10 % in most of the studied supersaturations. Depending mostly on the condensed-phase interactions between the organic molecules, material with solubilities larger than about 0.1–100 g L^{-1} could be treated as soluble in the CCN activation process over atmospherically relevant particle dry diameters and supersaturations. Our results indicate that understanding the details of the solubility distribution in the range of 0.1–100 g L^{-1} is thus critical for capturing the CCN activation, while resolution outside this solubility range will probably not add much information except in some special cases. The connections of these results to the previous observations of the CCN activation and the molecular properties of complex organic mixture aerosols are discussed. The presented results help unravel the mechanistic reasons behind observations of hygroscopic growth and CCN activation of atmospheric secondary organic aerosol (SOA) particles. The proposed solubility distribution framework is a promising tool for modeling the interlinkages between atmospheric aging, volatility and water uptake of atmospheric organic aerosol.

1 Introduction

Interactions of atmospheric aerosol particles with ambient water vapor determine to a large extent the influence that aerosols have on climate. On one hand, the water content of aerosol particles at atmospheric relative humidity (RH) below 100 % contributes significantly to the direct effect they have on the global radiative balance (Seinfeld and Pandis, 2006; Petters and Kreidenweis, 2007; Swietlicki et al., 2008; Zieger et al., 2011; Rastak et al., 2014). On the other hand, the water affinity of aerosol constituents, together with their dry size, defines the efficiency with which these particles can activate as cloud condensation nuclei (CCN) under supersaturated conditions (RH > 100 %), form cloud droplets, and thus affect the properties of clouds (Twomey 1974; Albrecht, 1989; McFiggans et al., 2006). To quantify the effects

of aerosol particles on clouds and climate, it is thus necessary to understand the ways that aerosol constituents interact with water.

Organic compounds contribute a large fraction (20–90 %, depending on the environment) of atmospheric submicron particulate mass (Jimenez et al., 2009) – which is the part of the aerosol size distribution that typically dominates the CCN numbers. A significant fraction of this organic aerosol (OA) is secondary – i.e., produced in the atmosphere from the condensation of oxidation products of volatile, intermediate volatility and semi-volatile organic compounds (VOCs, IVOCs and SVOCs). Emissions of biogenic VOCs such as monoterpenes, isoprene and sesquiterpenes, followed by their subsequent oxidation and condensation in the atmosphere, are thought to be the dominant source of secondary organic aerosol (SOA) on a global scale (Hallquist et al., 2009, and references therein) – although recent studies also suggest a notable anthropogenic component to the global SOA (Volkamer et al., 2006; Hoyle et al., 2011; Spracklen et al., 2011).

The solubility in water is one of the key properties governing the water absorption (i.e., hygroscopic growth) and CCN activation of aerosol particles. Together with aqueous-phase activity coefficients, surface tension, density and dry mass of the particle, water solubility affects the aerosol particle water content in thermodynamic equilibrium (Pruppacher and Klett, 1997; Seinfeld and Pandis, 2006; Topping and McFiggans, 2012). Atmospheric organic compounds have a wide range of solubilities (Raymond and Pandis, 2003; Chan et al., 2008; Psichoudaki and Pandis, 2013). OA is thus a complex mixture of molecules with different CCN behavior to pure compounds. To accurately predict the water content and CCN activation of atmospheric OA, information on the dissolution behavior and aqueous-phase interactions of these complex mixtures is needed.

Representation of the complexity of OA is a major challenge for atmospheric chemical transport models: OA consists of thousands of different compounds whose properties are poorly known (Golstein and Galbally, 2007; Hallquist et al., 2009; Kroll et al., 2011). Approaches that simplify the complex nature of the OA mixture, yet reproduce its behavior accurately enough, are required to be able to assess the climate and air quality effects of atmospheric organics in large-scale modeling applications. One example of such an approach is the representation of the condensation and evaporation of SOA using a limited number of surrogate compounds with a range of saturation concentrations, known as the volatility basis set (VBS, Donahue et al., 2006, 2011, 2012). Similar simplifying approaches are needed to represent the hygroscopic growth and CCN activation of OA as well.

When interpreting laboratory and field studies on hygroscopicity and CCN activation, a number of simplifying assumptions about the OA properties have been made, for instance, (1) assuming that organics completely dissolve in water at the point of activation (Huff-Hartz et al., 2006); (2) assuming a fraction ($\varepsilon_{\mathrm{eff}}$) of organics to be completely soluble and the remaining fraction ($1-\varepsilon_{\mathrm{eff}}$) completely insoluble in water (e.g., Pruppacher and Klett, 1997; Engelhart et al., 2008); and (3) lumping the phase-equilibrium thermodynamics, molar masses and densities of the OA constituents into a single semi-empirical parameter. One of the most commonly used formulations is the hygroscopicity parameter κ, which relates the water activity in the aqueous solution to the water and dry particle volumes, and can be modified to account for limited solubility as well if the solubilities of the individual aerosol constituents are known (Petters and Kreidenweis, 2007, 2008, 2013; Petters et al., 2009a–c; Farmer et al., 2015; see also Rissler et al., 2004, and Wex et al., 2007, for alternative single-parameter formulations). These common simplifications of organic aerosol solubility and hygroscopicity are summarized in Table 1.

Laboratory studies on different types of organic aerosols have provided important insights into the relationship between CCN activation, hygroscopic growth and water solubility of the atmospheric OA constituents. Raymond and Pandis (2002, 2003) and Chan et al. (2008) investigated the CCN activation of single-component and multicomponent aerosol particles consisting of organic compounds with known solubilities in water, and found that the particles activated at lower supersaturations than would have been expected based on the bulk solubility of their constituents. As an example, the laboratory studies by Chan et al. (2008) indicate that the CCN activation of material with water solubility as low as $1\,\mathrm{g\,L^{-1}}$ could be predicted assuming complete dissolution. For some model systems, the surface properties (wettability) of the aerosol particles, instead of the bulk water solubility, seemed a more important factor defining their CCN activation (Raymond and Pandis, 2002). Huff-Hartz et al. (2006) attributed part of this effect to residual water left in the particles upon their generation, causing the particles to exist as metastable aqueous solutions and thus activate at lower supersaturations than the corresponding dry material. The rest of the apparent increase in solubility was attributed to potential impurities in the particles. In general, the results reported by Huff-Hartz et al. (2006) suggested that compounds with water solubilities above $3\,\mathrm{g\,L^{-1}}$ behaved as if they were completely soluble in water, in general agreement with the earlier results of Hori et al. (2003).

Secondary organic aerosol particles generated in the laboratory through oxidation chemistry and condensation of the reaction products have also been found to activate as cloud droplets and thus contribute to the atmospheric CCN budgets (Cruz and Pandis, 1997, 1998; Huff Hartz et al., 2005; VanReken et al., 2005; Prenni et al., 2007; King et al., 2007, 2009; Engelhart et al., 2008, 2011; Asa-Awuku, 2009, 2010). These particles probably resemble the real atmospheric SOA more closely than individual organic species or their simple mixtures, but the theoretical interpretation of their CCN behavior is complicated by the variety of their constituents.

Table 1. Simplified descriptions of organic mixture solubilities.

Mixture model	Number of components	Solubility presentation	Other input parameters
Complete dissolution	1	$c_{sat} \rightarrow \infty^*$	M_{org}, ρ_{org}
κ	1	$\kappa(c_{sat}, M_{org}, \rho_{org})$	–
Soluble fraction ε_{eff}	2	$c_{sat,1} \rightarrow \infty \quad c_{sat,2} = 0$	M_{org}, ρ_{org}

* c_{sat} the solubility (saturation concentration) in aqueous solution.

Despite the fact that CCN activity of SOA has been reported to vary with the volatile precursor identity and loading (Varutbangkul et al., 2006; King et al., 2009; Good et al., 2010), photochemical aging (Duplissy et al., 2008; Massoli et al., 2010), and temperature (Asa-Awuku et al., 2009), the reported hygroscopicity parameter κ values determined for different SOA types are remarkably similar, being typically around 0.1 for the overall SOA and 0.3 for the dissolved fraction extracted from the aqueous sample (Asa-Awuku et al., 2010; King et al., 2010). Similarly, Huff Hartz et al. (2005) reported effective solubilities of as high as 100 g L^{-1} for both mono- and sesqui-terpene SOA – although both are known to consist of a range of compounds with different solubilities. These results demonstrate the importance of knowing the water-soluble fraction of SOA under varying conditions but suggest that its exact speciation is probably not necessary for predictive understanding of the CCN activity of SOA particles (Asa-Awuku et al., 2010; Engelhart et al., 2011). The κ values inferred from subsaturated or supersaturated conditions for the same SOA mixtures, on the other hand, are not always consistent, the subsaturated κ values being typically lower than the supersaturated ones (Prenni et al., 2007; Duplissy et al., 2008; Wex et al., 2009; Topping and McFiggans, 2012). Multiple possible reasons for this have been presented in the literature, including incomplete dissolution of the aerosol constituents under subsaturated conditions (Petters et al., 2009a), surface tension effects (Good et al., 2010), RH-driven effects on the reaction chemistry and thus the composition (solubility and activity) of the formed SOA (Poulain et al., 2010), evaporation and condensation of semi-volatile organic compounds (Topping and McFiggans, 2012), or the non-ideality of the mixtures being more pronounced under the subsaturated conditions (Kreidenweis et al., 2006; Petters et al., 2009a; Good et al., 2010).

While the basic theory of cloud droplet activation for pure water-soluble compounds is relatively well established (Pruppacher and Klett, 1997; Asa-Awuku et al., 2007; Topping and McFiggans, 2012; Farmer et al., 2015), and a number of theoretical and experimental studies on the different aspects controlling the CCN activation of SOA have been presented (see above, McFiggans et al., 2006; Dusek et al., 2006, and references therein), only a few of these studies have investigated the implications of the water solubilities of complex organic mixtures for CCN activation. Understanding the relationship between the dissolution behavior and CCN activation of complex organic mixtures is, however, needed to constrain the water-soluble fraction of SOA under varying conditions as well as to systematically unravel the mechanisms causing the apparent simplicity in the CCN behavior of complex organic mixtures.

In this work, we introduce a framework for representing the mixture components with a continuous distribution of solubilities, similar to the VBS (Donahue et al., 2006, 2011, 2012). Using this framework in a theoretical model, we investigate the dissolution behavior of complex organic mixtures and their CCN activity, focusing on the impact of mixture solubility on CCN activation. In particular, we study the response of the CCN activation to varying solubility ranges, distribution shapes, and numbers of components in the mixture. Furthermore, we compare the CCN-activation predictions using the simplified solubility representations outlined above (complete dissolution, soluble fraction ε_{eff}, and hygroscopicity parameter κ without including knowledge about the component solubilities) with the more detailed description using the full solubility distributions, and study the relationship of the simplified solubility parameters ε_{eff} and κ with the true mixture solubility distribution. Although the solubility ranges and other thermodynamic properties of the mixture have been chosen to represent SOA, many of the concepts and approaches introduced here can be applied to any particles consisting of complex mixtures of organic compounds with varying water solubilities. Finally, we discuss the applicability of the introduced framework for describing the water interactions of realistic SOA mixtures and the relevant future directions.

2 Methods

2.1 Theoretical predictions of CCN activation of complex organic mixtures

Figure 1 schematically summarizes the model system considered in this study. We consider a monodisperse population of spherical aerosol particles consisting of an internal mixture of organic compounds. When exposed to water vapor, these particles grow, reaching thermodynamic equilibrium between the water vapor and the particle phase. The wet particle is allowed to consist of maximum two phases: the insol-

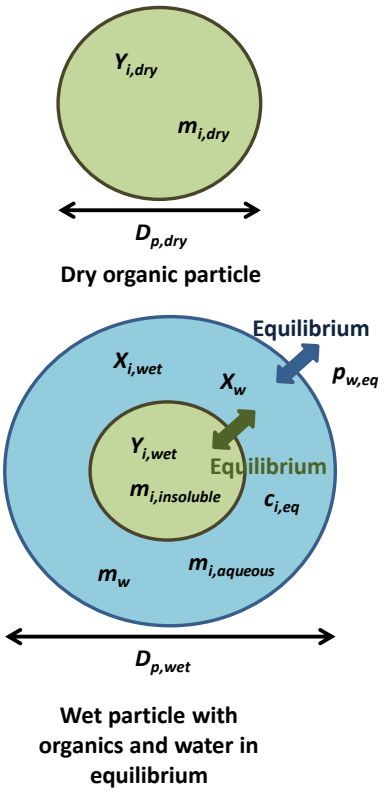

Figure 1. Schematic of the conceptual model used in the equilibrium composition calculations. The dry particle is assumed to consist of n organic compounds, each denoted with a subscript i. The wet particle is assumed to consist of a dry organic (insoluble) phase and an aqueous phase with water and dissolved organics. The aqueous phase is assumed to be in equilibrium with the ambient water vapor. Y refers to mole fractions in the organic phase, X to mole fractions in the aqueous phase, and m to the masses of the organic constituents and water. $c_{i,\mathrm{eq}}$ refers to the equilibrium concentration of each organic compound in the aqueous solution and $p_{\mathrm{w,eq}}$ to the equilibrium vapor pressure of water above the aqueous solution.

uble organic phase and the aqueous phase. The compositions of the organic and aqueous phases are determined on the one hand by the equilibrium between the aqueous phase and the water vapor, and on the other hand by the equilibrium of the aqueous phase with the organic insoluble phase. To isolate the effects of solubility from organic volatility effects, we do not allow the organics to evaporate from the droplet – i.e., we assume that the equilibrium vapor pressures of the organics are 0 above the droplet surface. Similarly, no condensation of organics from the gas phase to the particles is allowed to take place. The validity of this assumption depends on the gas-phase concentrations of the organic species as well as the atmospheric temperature during the cloud formation process. Testing it under different atmospherically relevant conditions deserves some future attention, accounting for the dynamics of the atmospheric gas phase as well (see also Topping and McFiggans, 2012). In this study, however, we focus strictly on the CCN-activation process. The organic composition and dry particle size were treated as an input to a model calculating the final equilibrium composition, wet size, and CCN activation behavior of these particles. Note that, while the solubility in the equations presented in the next Sects. 2.1 and 2.2 is non-dimensional ($\mathrm{g\,g^{-1}_{H_2O}}$), in the presentation of the results, it is converted into $\mathrm{g\,L^{-1}}$, assuming constant unit density of water.

2.1.1 Equilibrium between water vapor and an aqueous phase containing dissolved material

The Köhler equation (Pruppacher and Klett, 1997) is used to link the ambient water vapor saturation ratio S with the size, composition and water content of the aerosol particles in thermodynamic equilibrium (lower panel of Fig. 1):

$$S = \frac{p_{\mathrm{w,eq}}}{p_{\mathrm{w,sat}}} = a_{\mathrm{w}} \exp\left(\frac{4\sigma v_{\mathrm{w}}}{RT D_{\mathrm{p,wet}}}\right), \quad (1)$$

where $p_{\mathrm{w,eq}}$ (Pa) is the equilibrium vapor pressure of water over the droplet surface, $p_{\mathrm{w,sat}}$ (Pa) the saturation vapor pressure over a pure flat water surface, σ ($\mathrm{N\,m^{-1}}$) is the surface tension of the droplet, v_{w} the molar volume of water in the aqueous phase, M_{w} ($\mathrm{kg\,mol^{-1}}$) the molar mass of water, ρ ($\mathrm{kg\,m^{-3}}$) the density of the aqueous phase, $D_{\mathrm{p,wet}}$ (m) the diameter of the droplet, T (K) the temperature and R ($\mathrm{J\,mol^{-1}\,K^{-1}}$) the universal gas constant. a_{w} is the water activity, defined as the product of the water mole fraction X_{w} and water activity coefficient in the aqueous-phase Γ_{w}:

$$a_{\mathrm{w}} = X_{\mathrm{w}}\Gamma_{\mathrm{w}}. \quad (2)$$

The activity coefficient describes the interactions between water molecules and the dissolved organic molecules in the mixture. The saturation ratio at which the particles of dry size $D_{\mathrm{p,dry}}$ activate as cloud droplets (i.e., continue growing in size even if the saturation ratio decreases), is referred to as the critical saturation ratio S_{c}. Mathematically, this corresponds to the highest local maximum in the $S(D_{\mathrm{p,wet}})$ curve, usually referred to as the Köhler curve.

2.1.2 Equilibrium between the aqueous and insoluble organic phases

The composition of the droplet and the distribution of material between the organic insoluble and aqueous phases can be calculated by applying the principles of mass conservation and the thermodynamic equilibrium of the organic components in an aqueous mixture with the insoluble organic phase. As the mass transfer of organics between the particles and the gas phase is neglected, the total mass of the dry particle m_{dry}, being the sum over all components i, is equal to the total organic mass in the wet droplet (see Fig. 1):

$$m_{\mathrm{dry}} = \sum_i^n m_{i,\mathrm{insoluble}} + \sum_i^n m_{i,\mathrm{aqueous}}, \quad (3)$$

where n is the total number of organic compounds, $m_{i,\mathrm{insoluble}}$ is the mass of compound i in the insoluble organic phase and $m_{i,\mathrm{aqueous}}$ the mass of compound i in the aqueous phase. The same holds for each organic compound individually:

$$m_{i,\mathrm{dry}} = y_{i,\mathrm{dry}} m_{\mathrm{dry}} = m_{i,\mathrm{insoluble}} + m_{i,\mathrm{aqueous}}, \quad (4)$$

where $y_{i,\mathrm{dry}}$ is the mass fraction of i in the dry organic particle. On the other hand, the concentration of each organic compound in the aqueous phase is determined by the thermodynamics of the two-phase system consisting of the insoluble organic phase and the aqueous solution phase. The mass of each organic compound i in the aqueous phase can be expressed as (Prausnitz et al., 1998; Banerjee, 1984)

$$m_{i,\mathrm{aqueous}} = \begin{cases} \gamma_i Y_{i,\mathrm{wet}} c_{\mathrm{sat,pure},i} m_{\mathrm{w}} & Y_{i,\mathrm{wet}} > 0, \\ m_{i,\mathrm{dry}} & Y_{i,\mathrm{wet}} = 0, \end{cases} \quad (5)$$

where γ_i is the activity coefficient of i in the insoluble organic phase (where the reference state is the pure component dissolution to water), $Y_{i,\mathrm{wet}}$ and $c_{\mathrm{sat,pure},i}$ (here in g $\mathrm{g}^{-1}_{\mathrm{H_2O}}$) are the organic-phase mole fraction and pure component solubility (saturation concentration) of i, and m_{w} is the total mass of water in the droplet. The former equation corresponds to the situation where the particle contains an insoluble organic core in thermodynamic equilibrium, the latter to the case where only the aqueous phase exists; i.e., all the organic material has dissolved in the water. Although the mole fraction and the corresponding molar activity coefficient have been used in Eq. (5), a similar relationship can be defined using the mass fraction in the organic phase and a corresponding mass-based activity coefficient. For a multicomponent system in which the molar mass of the organic species varies, the mole and mass fractions of a given species are not necessarily equal. In this study, however, we assume a constant molar mass throughout the organic mixture for simplicity, leading to the mass and mole fractions in the organic phase to be the same; i.e., $Y_i = y_i$ for all compounds. All the equations presented below can be re-derived in a relatively straightforward manner taking into account a potential difference between the mole and the mass fractions in the organic phase.

Finding the organic- and aqueous-phase compositions that satisfy Eqs. (3)–(5) for given water and dry particle masses (m_{w} and m_{dry}, respectively) requires solving of n coupled equations. These equations were expressed using the ratio χ_i of organic compound i in the insoluble core of the wet particle to the total mass of the compound (Raymond and Pandis, 2003; Petters and Kreidenweis, 2008):

$$\chi_i = \frac{m_{i,\mathrm{insoluble}}}{m_{i,\mathrm{insoluble}} + m_{i,\mathrm{aqueous}}} = \frac{m_{i,\mathrm{insoluble}}}{m_{i,\mathrm{dry}}} = \frac{m_{i,\mathrm{insoluble}}}{Y_{i,\mathrm{dry}} m_{\mathrm{dry}}}. \quad (6)$$

The mole fraction (equal to the mass fraction for the mixtures considered here) of i in the insoluble core is defined as

$$Y_{i,\mathrm{wet}} = \frac{m_{i,\mathrm{insoluble}}}{\sum_i m_{i,\mathrm{insoluble}}} = \frac{\chi_i m_{i,\mathrm{dry}}}{\sum_i \chi_i m_{i,\mathrm{dry}}} = \frac{\chi_i Y_{i,\mathrm{dry}}}{\sum_i \chi_i Y_{i,\mathrm{dry}}}. \quad (7)$$

Finally, combining Eqs. (3)–(7), we get n equations of the form

$$\chi_i = 1 - \frac{\gamma_i \chi_i Y_{i,\mathrm{dry}} c_{i,\mathrm{sat,pure}} m_{\mathrm{w}}}{m_{i,\mathrm{dry}} \sum_i \chi_i Y_{i,\mathrm{dry}}}, \quad (8)$$

which can be solved for χ_i with the constraint $0 \le \chi_i \le 1$ for given water and dry particle masses.

2.1.3 Representation of complex organic mixtures: solubility distributions and thermodynamic properties

A novel aspect of this study as compared with previous theoretical work is the representation of complex mixtures using their aqueous solubility distribution of the individual species. In our calculations, we used mixtures of n compounds, whose water solubilities ranged from $c_{\mathrm{sat,min}}$ to $c_{\mathrm{sat,max}}$, either on a linear or logarithmic basis. The shape of the distribution could vary as well. In this work, we studied essentially three types of mass fraction distributions in the dry particle: a uniform distribution in which all solubilities are equally abundant, distribution increasing steadily (linearly or logarithmically), and a distribution decreasing steadily (linearly or logarithmically). The 72 studied solubility distributions are specified in Table 2, and the solubility distributions for $n = 10$, $c_{\mathrm{sat,min}} = 0.1\ \mathrm{g\,L^{-1}}$ and $c_{\mathrm{sat,max}} = 1000\ \mathrm{g\,L^{-1}}$ are presented in Fig. 2 as examples.

For simplicity, we assumed that water forms an ideal solution with the dissolved organics; i.e., $\Gamma_{\mathrm{w}} = 1$, thus yielding an activity equal to the mole fraction of water, $a_{\mathrm{w}} = X_{\mathrm{w}}$ in Eq. (1). Since information about the activity coefficients of organic species in purely organic mixtures is still scarce, we studied two alternative approaches to representing the dissolution thermodynamics of the SOA mixture in Eqs. (9)–(12): (1) assuming an ideal organic mixture where $\gamma = 1$ for all compounds in the insoluble phase; and (2) assuming a constant organic phase activity $\gamma_i Y_{i,\mathrm{wet}}$ of unity for all compounds – in which case the dissolution behavior of each i is similar to their behavior as pure components. These cases probably represent the limiting cases for the dissolution of SOA components in CCN activation reasonably well, the former representing a lower limit and the latter an upper limit

Table 2. Solubility distributions of the organic mixtures considered in this study.

Distribution[a]	Shape	Number of components	$[c_{sat,min}, c_{sat,max},]$[b] ($g\,L^{-1}$)
1	Flat, log c axis	3, 5, 10, 100	Low: $[10^{-5}, 10^{3}]$
2	Flat, linear c axis		
3	Log. increasing		Mid: $[0.1, 10^{3}]$
4	Linear increasing		
5	Log. decreasing		High: $[10, 10^{3}]$
6	Linear decreasing		

[a] For all solubility distributions, two assumptions about the organic-phase activity coefficients: (1) ideal mixture and (2) unity activity (see text for details); [b] c_{sat} the solubility (pure component saturation concentration) in aqueous solution.

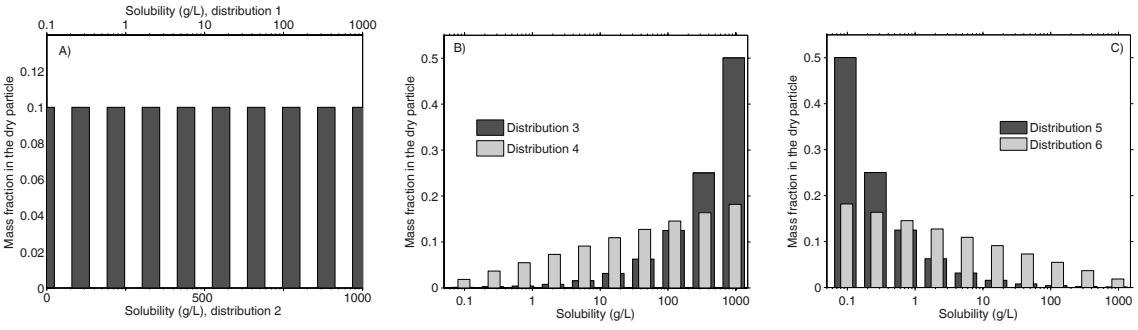

Figure 2. Examples of solubility distributions used in the calculations for saturation concentrations ranging from 0.1 to 1000 $g\,L^{-1}$. **(a)** Linear and logarithmic flat distributions; **(b)** linear and logarithmic increasing distributions; and **(c)** linear and logarithmic decreasing distributions. The numbers of the distributions refer to the numbering in Table 2 (see Sect. 2.1.4).

for the overall solubility of the dry particle. Applying the two limiting assumptions about the interactions of the compounds in the organic phase for the 72 different solubility distributions (Table 2) thus results in a total of 144 unique representative model mixtures.

The density, surface tension, and molar masses assumed for water and the organic compounds are summarized in Table 3. Although the density, surface tension and molar mass of the organics are likely to vary with the solubility, we kept them constant throughout the organic mixture to isolate the solubility effects on the CCN behavior. The values were chosen based on literature studies of the CCN behavior of SOA (Engelhart et al., 2011; Asa-Awuku et al., 2010). The surface tension σ was approximated by the surface tension of water, and the molar volume of water in the aqueous phase was assumed to be the same as for pure water. Furthermore, we assumed no dissociation of the organics in the aqueous phase.

2.1.4 Model calculations

We solved Eq. (8) for organic mixtures with Matlab internal function *fsolve*, for varying water and dry particle masses m_w and m_{dry}, covering 50 different dry particle diameters between 20 and 500 nm. The calculations yielded the composition of the insoluble organic and aqueous phases, and thus the mole fraction of water in the aqueous solution X_w. From these results, the Köhler curves $S(D_{p,wet})$ corresponding to each dry particle mass could be calculated using Eq. (1) (see Fig. 3a for an example of the Köhler curves). The critical supersaturations s_c (defined as $S_c - 1$) corresponding to specific dry particle diameters $D_{p,dry}$ (also termed activation diameters $D_{p,act}$ at a given saturation ratio S or supersaturation s) were determined from the maxima of the Köhler curves (see Fig. 3a). The temperature was assumed to be 298 K in all calculations. These calculations for the 144 unique organic model mixtures corresponded to 7200 Köhler curves yield-

Table 3. Properties of water and organic compounds used in Köhler curve calculations (see Eq. 1).

Property (unit)*	Water	Organic i
ρ ($kg\,m^{-3}$)	1000	1500
σ ($N\,m^{-1}$)	0.073	–
M($kg\,mol^{-1}$)	0.018	0.18

* These properties were chosen based on literature on the effective molar masses and densities determined for laboratory SOA (Engelhart et al., 2011; Asa-Awuku et al., 2010), and assumed to be same for every organic compound i.

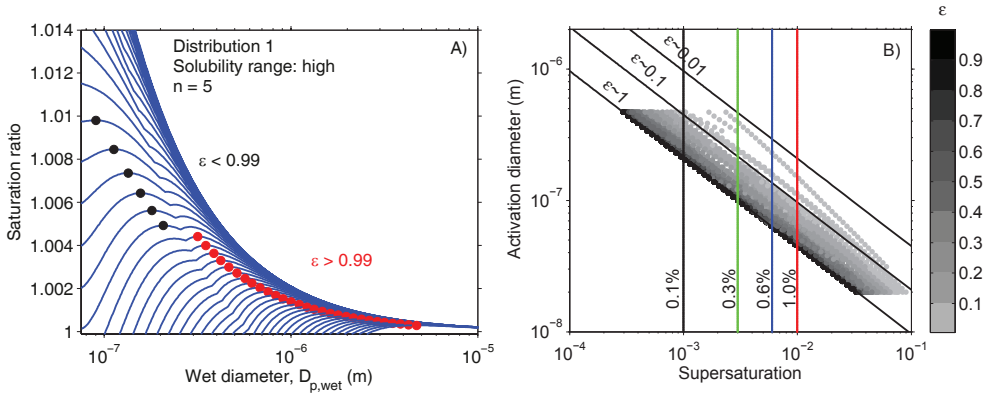

Figure 3. (a) Examples of Köhler curves for the flat logarithmically spaced solubility distribution (distribution 1 in Table 2) with $n = 5$ and the high solubility range (Table 2). The dots indicate the point of activation, black indicating incomplete dissolution ($\varepsilon < 1$) and red complete dissolution ($\varepsilon = 1$). **(b)** The activation points determined from the model calculations (in total, 7200 Köhler curves; see Table 2), corresponding to in total 5957 points in the activation dry diameter vs. supersaturation space. Also, the dependence of the dissolved fraction at the point of activation is illustrated.

ing 5957 ($D_{\mathrm{p,act}}$, s_{c}) pairs (activation points; see Fig. 3b). For the remaining 1143 curves, no activation points were found with the given combinations of mixture properties and dry diameters. For comparisons with the simple solubility representations, the dissolved organic fraction defined as

$$\varepsilon = \frac{\sum m_{i,\mathrm{aqueous}}}{m_{\mathrm{dry}}} \tag{9}$$

was extracted from the model output.

2.2 Comparison of the full model output to simple solubility representations

To investigate the performance of the simple solubility representations given in Table 1 in reproducing the CCN activation of complex mixtures, we fitted the ($D_{\mathrm{p,act}}$, s_{c}) data created by the full model using these simpler models. No fitting is required for the complete solubility approach. Using the obtained solubility parameters from the optimal fit and the corresponding simplified forms of the Köhler equation, we then recalculated new ($D_{\mathrm{p,act}}$, s_{c}) pairs and compared them to the predictions by the full model. Furthermore, we investigated the relationships between the true mixture solubility distribution and the simplified solubility parameters. The details of the approach used for each simple model are outlined below.

2.2.1 Complete dissolution

In the case where all of the organic material is assumed to completely dissolve at the point of activation, the calculation of the aqueous solution composition becomes trivial as

$$m_{i,\mathrm{dry}} = m_{i,\mathrm{aqueous}} \tag{10}$$

for all the compounds, and the water mole fraction can simply be calculated based on the dry particle mass as

$$X_{\mathrm{w}} = \frac{\frac{m_{\mathrm{w}}}{M_{\mathrm{w}}}}{\frac{m_{\mathrm{w}}}{M_{\mathrm{w}}} + \frac{m_{\mathrm{dry}}}{M_{\mathrm{org}}}}, \tag{11}$$

where m_{w} is the water mass in the droplet, m_{dry} the dry particle mass (related to $D_{\mathrm{p,dry}}$ through the organic density ρ_{org}) and M_{org} the organic molar mass. The X_{w} calculated in this way was inserted into Eq. (1) to yield the corresponding ($D_{\mathrm{p,act}}$, s_{c}) predictions and was also applied to calculate the solution density and surface tension as mass-weighted averages of the water and pure organic values.

2.2.2 Hygroscopicity parameter κ

In many practical applications, the water activity and the difference in the densities and molar masses of water and the dry material are expressed with a single hygroscopicity parameter κ, introduced by Petters and Kreidenweis (2007), defined as

$$\frac{1}{a_{\mathrm{w}}} = 1 + \kappa \frac{V_s}{V_{\mathrm{w}}}, \tag{12}$$

where V_s and V_{w} are the volumes of the dry material and water, respectively. The following formulation of the relationship between water saturation ratio, aerosol size and composition is referred to as the κ-Köhler equation:

$$S = \frac{D_{\mathrm{p,wet}}^3 - D_{\mathrm{p,dry}}^3}{D_{\mathrm{p,wet}}^3 - D_{\mathrm{p,dry}}^3(1-\kappa)} \exp\left(\frac{4\sigma M_{\mathrm{w}}}{RT\rho D_{\mathrm{p,wet}}}\right), \tag{13}$$

yielding an approximate expression for the relationship between s_{c} and $D_{\mathrm{p,act}}$ defined as

$$s_{\mathrm{c}} = \frac{2}{3}\left(\frac{4M_{\mathrm{w}}\sigma}{RT\rho}\right)^{\frac{3}{2}} \left(3\kappa D_{\mathrm{p,act}}^3\right)^{\frac{-1}{2}}. \tag{14}$$

Equation (14) was fitted to all ($D_{\mathrm{p,act}}$, s_{c}) data produced for a given organic mixture composition (see Table 2) by the full model, thus assuming a constant κ value for a given organic mixture. To mimic the application of Eq. (14) to experimental data with no knowledge of the exact solute composition, in this case we assumed the surface tension and density to be those of water when fitting the κ values to the full model data. The above formulation of κ, which is often used in the interpretation of experimental data as well, thus contains information about solubility, potential aqueous-phase non-ideality, as well as molar mass and density of the solutes (see Farmer et al., 2015).

2.2.3 Soluble fraction $\varepsilon_{\mathrm{eff}}$

For an ideal solution of water and an organic solute, the κ is directly proportional to the dissolved fraction and the ratio of the molar volumes of water and the solute; i.e., $\kappa = \varepsilon\kappa_{\max}$, where $\kappa_{\max} = (M_{\mathrm{w}}/M_{\mathrm{org}})(\rho_{\mathrm{org}}/\rho_{\mathrm{w}})$. Assuming that a single soluble fraction $\varepsilon_{\mathrm{eff}}$ can represent a given organic mixture (see Table 2) at all considered supersaturations, substituting these relationships into Eq. (16) yields

$$s_{\mathrm{c}} = \frac{2}{3}\left(\frac{4M_{\mathrm{w}}\sigma}{RT\rho}\right)^{\frac{3}{2}}\left(3\frac{M_{\mathrm{w}}}{M_s}\frac{\rho_s}{\rho_{\mathrm{w}}}\varepsilon_{\mathrm{eff}}D_{\mathrm{p,act}}^3\right)^{\frac{-1}{2}}, \tag{15}$$

the corresponding form of the Köhler equation being (see Huff Hartz et al., 2005)

$$S = \frac{M_{\mathrm{org}}\rho_{\mathrm{w}}(D_{\mathrm{p,wet}}^3 - D_{\mathrm{p,dry}}^3)}{D_{\mathrm{p,wet}}^3(M_{\mathrm{org}}\rho_{\mathrm{w}}) + D_{\mathrm{p,dry}}^3(\varepsilon_{\mathrm{eff}}M_{\mathrm{w}}\rho_{\mathrm{org}} - M_{\mathrm{org}}\rho_{\mathrm{w}})} \times \exp\left(\frac{4\sigma M_{\mathrm{w}}}{RT\rho D_{\mathrm{p,wet}}}\right). \tag{16}$$

Again, we fitted Eq. (17) to the data produced by the full model and assumed the aqueous solution density and surface tension to be equal to those of water. When $\varepsilon_{\mathrm{eff}} < 1$, the following relationship has been used to estimate the effective saturation concentration of the mixture (Raymond and Pandis, 2002; Huff Hartz et al., 2005)

$$c_{\mathrm{sat,eff}} = \frac{\rho_{\mathrm{w}}(D_{\mathrm{p,wet}}^3 - D_{\mathrm{p,act}}^3)}{\varepsilon_{\mathrm{eff}}\rho_{\mathrm{org}}D_{\mathrm{p,act}}^3}. \tag{17}$$

2.2.4 Connection between $\varepsilon_{\mathrm{eff}}$ and the solubility distribution of the mixture

Let us now assume that the dissolved fraction at the point of activation for each considered mixture can be expressed as a sum of two terms, the contribution from the compounds below a threshold solubility bin i_{t} and the contribution from the compounds over the threshold:

$$\varepsilon = \frac{\sum_{i=1}^{i_{\mathrm{t}}} m_{i,\mathrm{aqueous}} + \sum_{j=i_{\mathrm{t}}+1}^{n} m_{j,\mathrm{aqueous}}}{m_{\mathrm{dry}}} = \frac{\sum_{i=1}^{i_{\mathrm{t}}} m_{i,\mathrm{aqueous}} + \left(\sum_{j=i_{\mathrm{t}}+1}^{n} m_{j,\mathrm{dry}} - \sum_{j=i_{\mathrm{t}}+1}^{n} m_{j,\mathrm{insoluble}}\right)}{m_{\mathrm{dry}}}. \tag{18}$$

We now hypothesize that assuming a single soluble fraction for a given aerosol mixture is in fact equivalent to assuming that everything above i_{t} is completely dissolved while all the material below this threshold remains undissolved, i.e.,

$$\varepsilon_{\mathrm{eff}} = \frac{\sum_{j=i_{\mathrm{t}}+1}^{n} m_{j,\mathrm{dry}}}{m_{\mathrm{dry}}}. \tag{19}$$

On the other hand, $\varepsilon = \varepsilon_{\mathrm{eff}}$ if the following condition is fulfilled (see Eq. 20):

$$\sum_{i=1}^{i_{\mathrm{t}}} m_{i,\mathrm{aqueous}} = \sum_{j=i_{\mathrm{t}}+1}^{n} m_{j,\mathrm{insoluble}} = \sum_{j=i_{\mathrm{t}}+1}^{n} m_{j,\mathrm{dry}} - \sum_{j=i_{\mathrm{t}}+1}^{n} m_{j,\mathrm{aqueous}}. \tag{20}$$

Substituting Eq. (5) into Eq. (20), we now have

$$F_{\mathrm{w}}\sum_{i=1}^{i_{\mathrm{t}}}\gamma_i Y_{i,\mathrm{wet}}c_{\mathrm{sat,pure},i} = \sum_{j=i_{\mathrm{t}}+1}^{n} Y_{\mathrm{dry},j} - F_{\mathrm{w}}\sum_{j=i_{\mathrm{t}}+1}^{n}\gamma_j Y_{j,\mathrm{wet}}c_{\mathrm{sat,pure},j}, \tag{21}$$

where

$$F_{\mathrm{w}} = \frac{m_{\mathrm{w}}}{m_{\mathrm{dry}}}. \tag{22}$$

At the limit of large n and in the case of a symmetric distribution of material between the insoluble organic and aqueous phases, Eq. (21) is satisfied by setting the threshold solubility i_{t} so that

$$\lim_{i\to i_{\mathrm{t}}} F_{\mathrm{w}}\gamma_i Y_{i,\mathrm{wet}}c_{\mathrm{sat,pure},i} = Y_{\mathrm{dry},i_{\mathrm{t}}} - F_{\mathrm{w}}\gamma_i Y_{i,\mathrm{wet}}c_{\mathrm{sat,pure},i}. \tag{23}$$

In this case, the threshold solubility c_{t} is found from the bin for which

$$c_{\mathrm{sat,pure},i_{\mathrm{t}}} = c_{\mathrm{t}} \approx \frac{Y_{\mathrm{dry},i_{\mathrm{t}}}}{Y_{\mathrm{wet},i_{\mathrm{t}}}} \times \frac{1}{\gamma_{i_{\mathrm{t}}}} \times \frac{1}{2F_{\mathrm{w}}}. \tag{24}$$

This is also equal to the bin where 50 % of the material is partitioned in the insoluble phase, i.e.,

$$\chi_{i_{\mathrm{t}}} = \frac{m_{i_{\mathrm{t}},\mathrm{insoluble}}}{m_{i_{\mathrm{t}},\mathrm{insoluble}} + m_{i_{\mathrm{t}},\mathrm{aqueous}}} = \frac{1}{1 + \frac{m_{i_{\mathrm{t}},\mathrm{aqueous}}}{m_{i_{\mathrm{t}},\mathrm{insoluble}}}} = \frac{1}{2}. \tag{25}$$

Finding the solubility threshold c_t requires knowledge of the ratio F_w (Eq. 22). F_w, on the other hand, depends on the ambient supersaturation and the total soluble mass – thus introducing a supersaturation dependence to the ε given by Eq. (18) as well. The magnitude of F_w as a function of supersaturation can be estimated by substituting Eqs. (15) and (17) into the definition of F_w (Eq. 22), which, after some rearranging, yields

$$F_w = \frac{\rho_w}{\rho_{org}}\left(\frac{2\varepsilon}{s_c} \times \frac{\rho_{org}}{\rho_w} \times \frac{M_w}{M_{org}} - 1\right) = \frac{\rho_w}{\rho_{org}}\left(\frac{2\varepsilon\kappa_{max}}{s_c} - 1\right). \quad (26)$$

3 Results

Figure 3a displays examples of the Köhler curves obtained from solving Eqs. (1) and (6) for distribution 1 (the flat logarithmic distribution) with varying solubilities and $n = 5$, assuming that the organics form an ideal mixture with each other. Each curve corresponds to a different dry size, and the dots indicate the activation point (S_{crit} corresponding to the activation dry diameter $D_{p,act}$). Black dots indicate incomplete dissolution ($\varepsilon < 0.99$) at the point of activation, while red dots indicate that in practice all the organics are dissolved into the aqueous phase at the point of activation ($\varepsilon > 0.99$). Qualitatively similar behavior was observed for all the considered distributions: as the overall solubility of the mixture increases, the dissolution of the compounds increases, leading eventually to complete dissolution at the point of activation. The transition from a regime with two phases (aqueous + insoluble) to a single aqueous phase is visible in the two maxima in Fig. 3a, in accordance with Shulman et al. (1996) and Petters and Kreidenweis (2008).

Figure 3b illustrates the parameter space probed in this study, showing the 5957 (s_{crit}, $D_{p,act}$) points corresponding to the Köhler curve maxima calculated for all the considered organic mixtures. The relationships between the critical supersaturation, activation diameter, and dissolved fraction ε at the point of activation are also schematically shown. The chosen dry diameters and supersaturations represent a conservative range of typical atmospheric conditions – as the total aerosol number concentrations are dominated by ultrafine (diameters smaller than 100 nm) particles at most locations. In most considered cases, the dissolved fractions fall between 0.1 and 1, but the lowest dissolved fractions at the point of activation are on the order of only a few percent – thus mimicking nearly insoluble aerosols. Therefore, the cases considered here represent a reasonable sample of atmospherically relevant conditions and SOA mixture compositions. The water-to-organic mass ratios F_w corresponding to the probed conditions and mixtures (see Sect. 2.2.4) range from values below 1 up to 1000, with most values around 10–100. In many of the following plots and considerations, we have chosen four

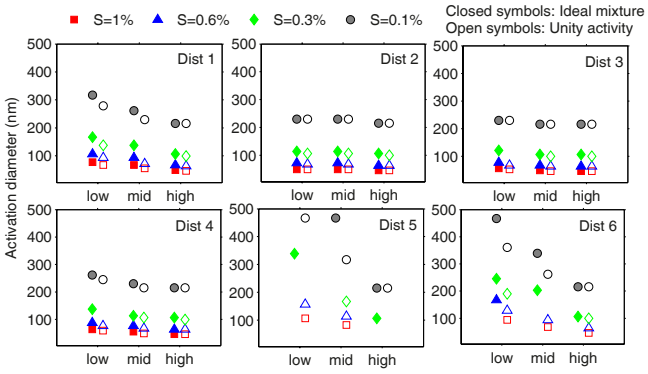

Figure 4. The dependence of the activation diameter for four different supersaturations ($s = 1$, 0.6, 0.3 and 0.1 %; see also Fig. 3b) on the solubility range for the solubility distributions outlined in Table 2 for $n = 5$, and the two assumptions about the organic-phase activity.

specific supersaturations, 0.1, 0.3, 0.6 and 1 %, as representative values for typical laboratory experiments, which are also indicated in Fig. 3b.

An example of the dependence of the activation diameter $D_{p,act}$ on the solubility range for all the studied distributions (see Table 2) and $n = 5$ is presented in Fig. 4. As expected, the activation diameter decreases with increasing supersaturation and solubility range for a given solubility distribution. The solubility distribution is reflected in the overall magnitude of the activation diameters: the distributions that have larger fractions of material at the higher end of the solubility range (distributions 2, 3, and 4) have generally lower activation diameters for a given supersaturation as compared with the other distributions. The case when unity activity in the organic phase is assumed results in smaller activation diameters for the same supersaturation as compared with the ideal organic mixture case (see Sect. 2.1.3 for the definitions of the cases).

Figure 5 presents the activation diameters predicted using the simplified solubility descriptions (Table 1) based on best fits to all available data as compared with the full description of the solubility distributions (Table 2). The results clearly show, not surprisingly, that assuming complete dissolution for all the mixtures consistently under-predicts the activation diameters (Fig. 5a). Representing the dissolution behavior with only one additional parameter, i.e., the hygroscopicity parameter κ (Eqs. 15 and 16) or the effective soluble fraction ε_{eff} (Eqs. 17 and 18), improves the agreement between the activation diameters considerably (Fig. 5b and c). Adding the knowledge about the molar mass and density of the organic mixture, which is the only difference between using the ε_{eff} instead of the single κ, adds only marginal improvements in predicting the activation diameters for a given supersaturation. The disagreements between the simplified models and the full theoretical treatment are largest for the smallest supersaturations. These are the cases with the widest range of

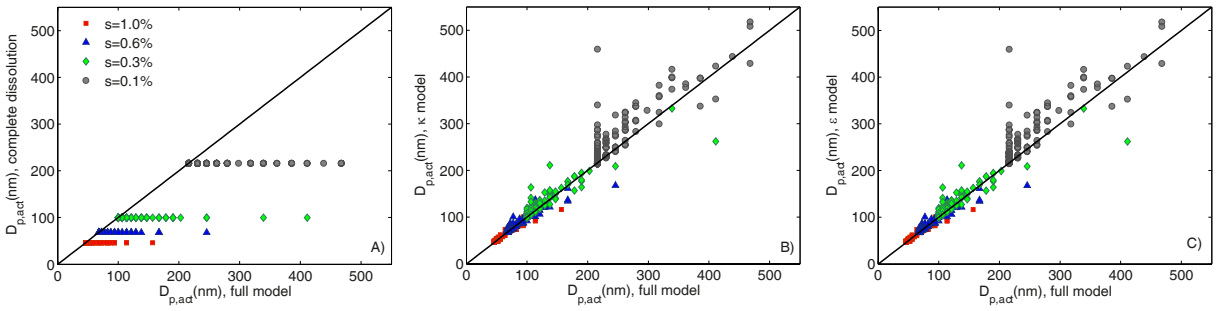

Figure 5. The activation diameter calculated using the solubility distributions (Table 2, referred to as the full model) and the simplified dissolution descriptions (Table 1): **(a)** complete dissolution assumption; **(b)** the hygroscopicity parameter κ; and **(c)** the soluble fraction $\varepsilon_{\mathrm{eff}}$ to describe the solubility of the organic mixture. The symbols correspond to the best fits to the full model data. The black line shows the 1 : 1 correspondence between the two data sets.

possible ε values at the point of activation (see Fig. 3b), and the effect is most obvious for the complete dissolution model: the larger the deviation from complete dissolution at the point of activation (i.e., the $\varepsilon \sim 1$ case in Fig. 3b), the more significant error we introduce. The activation diameters predicted assuming complete dissolution are within 10 % of the correct values if the real dissolved fraction ε is larger than about 0.7–0.8 at the point of activation.

The performance of the simple solubility models for all the studied Köhler curves is summarized in Fig. 6: while the complete dissolution assumption results in systematic underprediction (up to 40 %) of the activation diameter, the κ- and $\varepsilon_{\mathrm{eff}}$-based models are generally within 10 % (in most cases within 5 %) of the activation diameter predicted for the full solubility distribution representation.

Figure 7 compares the fitted parameters representing the mixture dissolution to the corresponding values inferred from the full mixture data for the 144 different mixtures. In Fig. 7a, the effective soluble fractions $\varepsilon_{\mathrm{eff}}$ are compared to the actual dissolved fractions ε at the point of activation for all the studied mixtures. While in the fits a single constant $\varepsilon_{\mathrm{eff}}$ has been assumed to represent a given mixture (see Eqs. 15 and 16), in reality, ε varies with supersaturation (Eq. 9). Thus, while the fitted $\varepsilon_{\mathrm{eff}}$ for a given mixture correlates very well with the average ε over all activation points (the markers in Fig. 7a), the performance of the approach can vary considerably with supersaturation (the grey lines in Fig. 7a). In practice, this means that describing a given complex mixture with a fixed soluble fraction yields representative average dissolution behavior, but does not guarantee correct solubility description for a specific s_{c} if fitted over a range of supersaturations. The corresponding comparison for the hygroscopicity parameter κ values describing the data is shown in Fig. 7b. A clear correlation between the fitted κ and the average ε is observed as expected (see Sect. 2.2.3), but the variation of ε with supersaturation again adds scatter to the data – suggesting a dependence of κ on s_{c}. The maximum κ, on the other hand, is defined primarily by the molar masses and densities of the organics. For our mixtures with

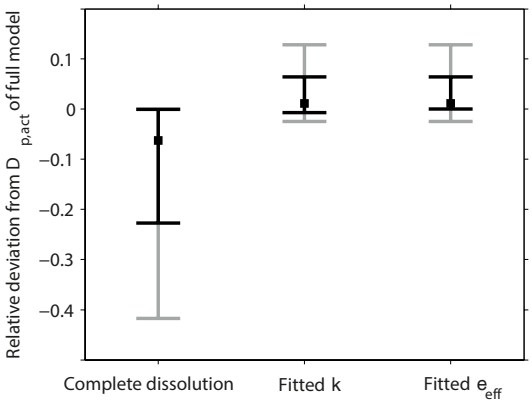

Figure 6. The performance of the simplified solubility representations (see Table 1) in predicting the activation diameter for a given supersaturation as compared with the full model. The black bars depict the 25th and 75th percentiles and the grey bars the 10th and 90th percentiles.

constant M_{org} and ρ_{org}, the value of κ_{max} is 0.15, which is indicated in Fig. 7b. The points above this theoretical maximum are a result of using the pure water density instead of the mixture value in the Kelvin term of the Köhler equation (Eq. 16). These results thus suggest that the κ values of 0.1–0.2 typically observed for SOA particles (Duplissy et al., 2011) are controlled by the molar masses and densities of the SOA mixtures to a large extent and can result from quite different SOA mixtures in terms of their solubilities.

To illustrate the relationship of the fitted $\varepsilon_{\mathrm{eff}}$ with the dissolution of a given mixture, the partitioning between the aqueous and insoluble organic phases is presented in Fig. 8 for distribution 1 with the "low" solubility range and $n = 100$ at the point of activation when $s_{\mathrm{c}} = 0.1$ % (see Table 2). Figure 8a shows the partitioning for the case where ideal organic mixture has been assumed and Fig. 8b shows the corresponding data for the unity activity case (see Eq. 5). The point of 50 % partitioning (c_{t}, Eqs. 20 and 21) is also shown. As described in Sect. 2.2.4, we expect c_{t} to be a reasonable

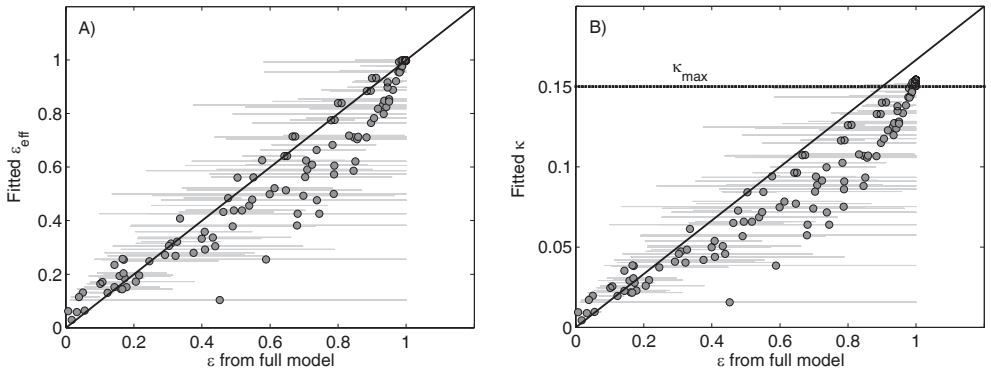

Figure 7. (a) The fitted soluble fraction $\varepsilon_{\mathrm{eff}}$ as function of the true dissolved fraction ε for each considered mixture (see Table 2). Symbols: mean ε over all activation points. Grey lines: the range of ε values at the different activation points for a given mixture. **(b)** The fitted κ values as a function of the true dissolved fraction ε for each considered mixture. The red dashed line denotes the limit of $\kappa_{\mathrm{max}} = 0.15$ that applies to all the studied mixtures. 1 : 1 lines are also indicated.

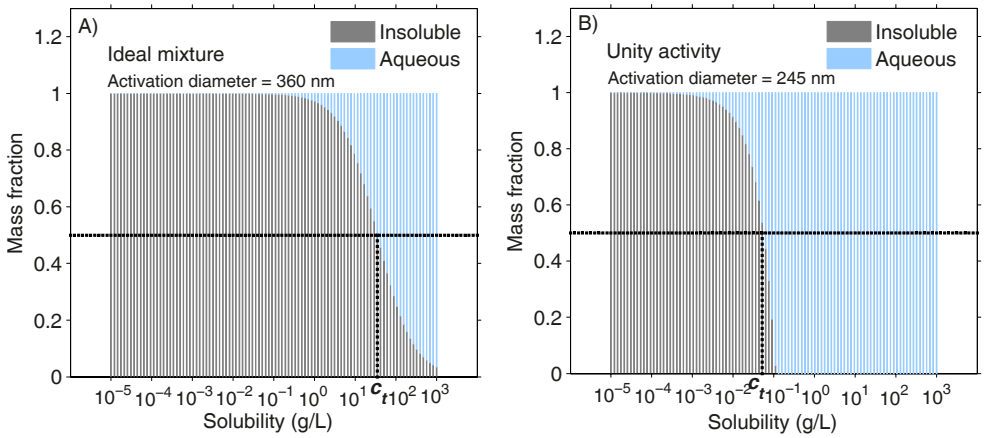

Figure 8. The dissolution behavior of the organic mixture corresponding to distribution 1 with $n = 100$ and the low solubility range (see Table 2) at the activation point for $s_{\mathrm{c}} = 0.1\,\%$ (see Fig. 4). The figures depict the distribution of material in each solubility bin between the aqueous and insoluble organic phases for the two different assumptions about the organic-phase activity. c_{t} refers to the 50 % point of the partitioning (Eqs. 24 and 25). **(a)** The ideal organic mixture. **(b)** The unity activity assumption.

estimate for the limit for complete dissolution, if the complex mixture is reduced to a two-component mixture of completely soluble and insoluble components. It should be noted, however, that the water content and ε of the droplet at the point of activation depend on supersaturation (see Eq. 25), also causing a dependence between c_{t} and s_{c}. Furthermore, Fig. 8 illustrates a difference in the solubility dependence of the partitioning behavior for the two organic activity assumptions. The ideal mixture displays a symmetrical sigmoidal dependence around c_{t}. For the unity activity case, on the other hand, the undissolved fraction is asymmetric around the 50 % value – dropping rapidly to 0 above c_{t} but approaching 1 asymptotically below c_{t}.

Figure 9 shows the distributions of the solubility bins containing the 50 %-partitioning points (c_{t}, Eqs. 20 and 21) on a decadal basis for all the activation points studied, illustrating also the differences between the two assumptions about the organic-phase activity. The c_{t} values for the ideal organic mixture (Fig. 9a, based on 2465 points) display a symmetrical distribution around the median value of about $10\,\mathrm{g\,L^{-1}}$. Also, a modest dependence of c_{t} on the number of components is observed: the cases with three and five components display slightly higher c_{t} values as compared with the cases with larger n. This apparent dependence is probably due to the discrete nature of the solubility distributions in combination with the fact that, for the different solubility ranges (see Table 2), only the lower end of the distribution is changed, while the upper end is always at $1000\,\mathrm{g\,L^{-1}}$. The unity activity case displays a much stronger n dependence (Fig. 9b, based on 3492 points): if analyzed separately, the median c_{t} shifts from about 0.1 to $10\,\mathrm{g\,L^{-1}}$ when n changes from 100 to 10 and 5, and up to $100\,\mathrm{g\,L^{-1}}$ for $n = 3$. Unlike the ideal mixture, this behavior is explained by the actual dissolution thermodynamics: in a system where the components do not

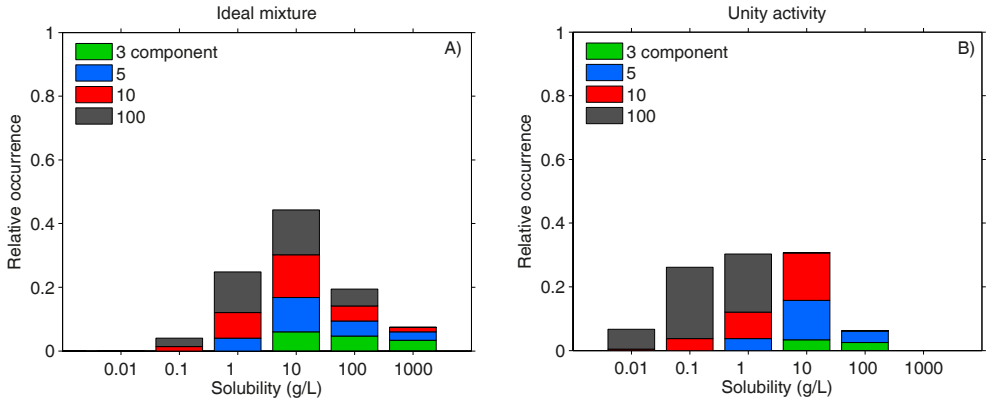

Figure 9. The distributions of the c_t values (i.e., the 50 % partitioning point; see Eqs. 24 and 25) at the point of activation for all the considered mixtures (Table 2) and activation points, and the two assumptions about the organic-phase activity. **(a)** The ideal organic mixture. **(b)** The unity activity assumption.

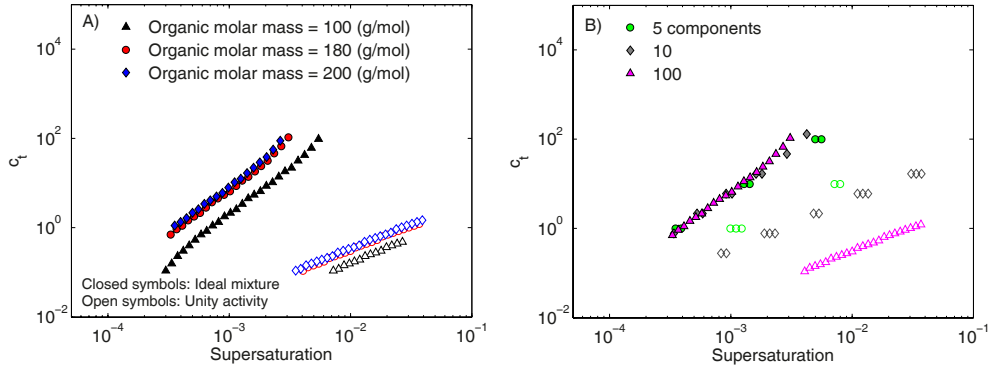

Figure 10. Sensitivity of the c_t values to supersaturation, molar mass and number of components for distribution 1 with the mid solubility range (see Table 2). Only points with limited solubility ($0 < \varepsilon < 1$) at the point of activation are included.

affect each other's solubility directly (i.e., the dissolution of a compound i is only limited by its own presence in the aqueous phase), the amount of dissolved material is only dependent on the total water content and is larger than the number of dissolvable components. If all the different mixtures are integrated together, the median c_t for the unity activity assumption lies at about 1 g L^{-1} – a decade lower than for the ideal mixture case. Figure 10 provides a more detailed look at the sensitivity of c_t to supersaturation, n and molar mass for one of the distributions (distribution 1, mid solubility range; see Table 2). As expected, c_t depends considerably on supersaturation. It can also be seen that, while c_t shows some sensitivity to the number of components (in line with Fig. 9) and molar mass, in our case, by far the most critical assumption is related to the organic mixture thermodynamics.

The fitted ε_{eff} values are compared in Fig. 11 to the fraction of mass with solubilities above the median c_t for the 134 mixtures that activated under the probed conditions, individually for both organic activity assumptions. The fitted dissolved fraction corresponds well to the fraction of mass with solubilities above the 50 %-partitioning point, as predicted by the theoretical principles outlined in Sect. 2.2.4. Also, the solubilities of the different distributions with varying shapes, numbers of components and solubility ranges can be represented reasonably well with a single median c_t (equal to 10 g L^{-1} for the ideal mixture case and 1 g L^{-1} for the unity activity case; see Fig. 9), with median deviations between the fitted ε_{eff} and the fraction above c_t of 9 and 8 %, respectively. On the other hand, these results indicate that the soluble fractions determined from experimental data on CCN activation provide information about the fraction of material with solubility above c_t. There are eight points that do not seem to follow the general trend, however: a group of points with all the material above the threshold solubility can display a variety of fitted ε_{eff} values. These are all points that correspond to the "high" solubility ranges. Distributions 5 and 6 (see Table 2) with $n = 3$ are among these points for both organic activity assumptions. For the ideal mixture case, distribution 1 with three components also diverges from the general trend, and for the unity activity assumption, distribution 5 falls into the category regardless of the number of components. These

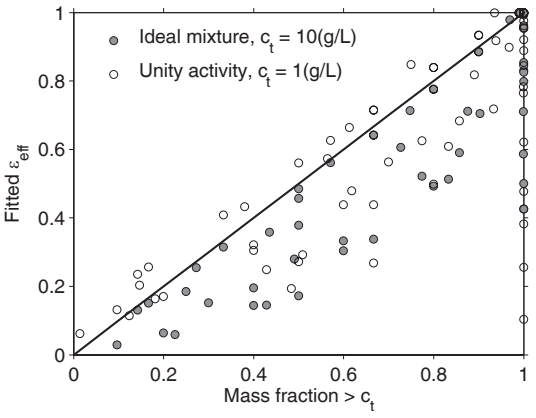

Figure 11. The relationship between the fitted dissolved fraction $\varepsilon_{\mathrm{eff}}$ at the point of activation and the mass fraction over the median c_{t} for all the considered mixtures and $s = 1$, 0.6, 0.3 and 0.1 %. Closed symbols: the ideal organic mixture assumption (median $c_{\mathrm{t}} = 10\,\mathrm{g\,L^{-1}}$). Open symbols: the unity activity assumption for the organics (median $c_{\mathrm{t}} = 1\,\mathrm{g\,L^{-1}}$).

points thus contribute to the high ends of the c_{t} distributions in Fig. 9.

The deviations in the activation diameters as predicted by the three simplified solubility representations (complete dissolution, ε and κ) are displayed in Fig. 12 as a function of the mixture properties for $s_{\mathrm{c}} = 0.1$, 0.3, 0.6 and 1 %. Again, the two different assumptions about the organic-phase activity are treated separately due to their different limiting solubilities c_{t} (Fig. 9) and different shapes of the partitioning distributions (Fig. 8). Also, the points close to complete dissolution at the point of activation ($\varepsilon \geq 0.8$; see Fig. 5 and its explanation in the text) are presented with a different color (grey symbols) than the points where the activation diameter differs significantly from the complete dissolution prediction ($\varepsilon < 0.8$, black symbols). As expected, the complete dissolution assumption performs better for the more water-soluble organic mixtures. Figure 12a and b illustrates this by showing the relationship between the norm of the error in the predicted $D_{\mathrm{p,act}}$ and the fraction of material below the median c_{t} (10 and $1\,\mathrm{g\,L^{-1}}$) for the two organic activity assumptions. The larger the amount of material below the solubility limit, the larger the deviation from the full model predictions. For the κ and ε models, on the other hand, the variable best correlating with the error in $D_{\mathrm{p,act}}$ induced by the simplification is different for the different organic activity assumptions – although close to complete dissolution, these models also do well, nearly independent of the solubility of the distribution. For the ideal mixture case, the fraction of mass between 1 and $100\,\mathrm{g\,L^{-1}}$ correlates better with the error (Fig. 12c, e) than the mass fraction below any solubility limit (not shown), while for the unity activity case, the material at the low end of the distribution (mass fraction below $1\,\mathrm{g\,L^{-1}}$) performs better (see Fig. 12d, f). The reason for this lies in the different shapes of the partitioning distributions resulting from the two assumptions (Fig. 8). For the symmetric partitioning curve of the ideal mixture case, the predicted ε and κ are most sensitive to differences in the partitioning behavior between compounds within the range of c_{t} corresponding to the supersaturation and particle diameter ranges studied here, i.e., 1–$100\,\mathrm{g\,L^{-1}}$ (see Fig. 12c, e). Anything outside these boundaries will behave as completely soluble or insoluble throughout the studied supersaturation space, thus not introducing a significant error when constant ε is assumed to describe the mixture. However, the more material that can behave as either insoluble or soluble, depending on the conditions, the larger the error we introduce by assuming a constant ε for a given mixture under any conditions. The story is different for the unity activity case (Fig. 12d, f): as the shape of the partitioning distribution (Fig. 8) does not depend on c_{t}, the compounds with solubilities below c_{t} will contribute relatively much more to the fitted $\varepsilon_{\mathrm{ff}}$ than for the previous case, and thus the more material there is in the "tail" of the partitioning distribution, the worse the assumption about a single ε for the whole distribution.

To relate the theoretical work conducted here to realistic atmospheric organic aerosol mixtures, Fig. 13 displays an example of a solubility distribution representing SOA formed from dark ozonolysis of α-pinene (Chen et al., 2011). The solubilities have been estimated with SPARC (see Wania et al., 2014, and references therein). The average molar masses and O : C ratios in each solubility bin are also displayed, along with the c_{t} values corresponding to the activation points with limited solubility – assuming that the organics form an ideal mixture with each other. Most of the material is predicted to have solubilities between 1 and $100\,\mathrm{g\,L^{-1}}$, indicating that this fresh α-pinene SOA is at the critical range of solubilities for limited dissolution at the point of activation. This in turn suggests that the observed difference between the κ values inferred from hygrosopicity and CCN activation for this mixture might largely result simply from the distribution of solubilities present.

4 Discussion and conclusions

We have studied the relationship between CCN activation and the solubility of 144 different theoretically constructed complex organic mixtures using Köhler theory, accounting for the partial solubility of the compounds in water and assuming ideal interactions between the dissolved molecules and water. The mixtures encompassed a wide variety of solubilities, and were represented by solubility distributions with various solubility ranges and shapes (analogously to the volatility basis set, VBS). Two limiting assumptions (ideal mixture vs. unity activity) about the interactions between the organics in the insoluble organic phase were tested. The results using this comprehensive solubility representation (termed "the full model") were compared to commonly used

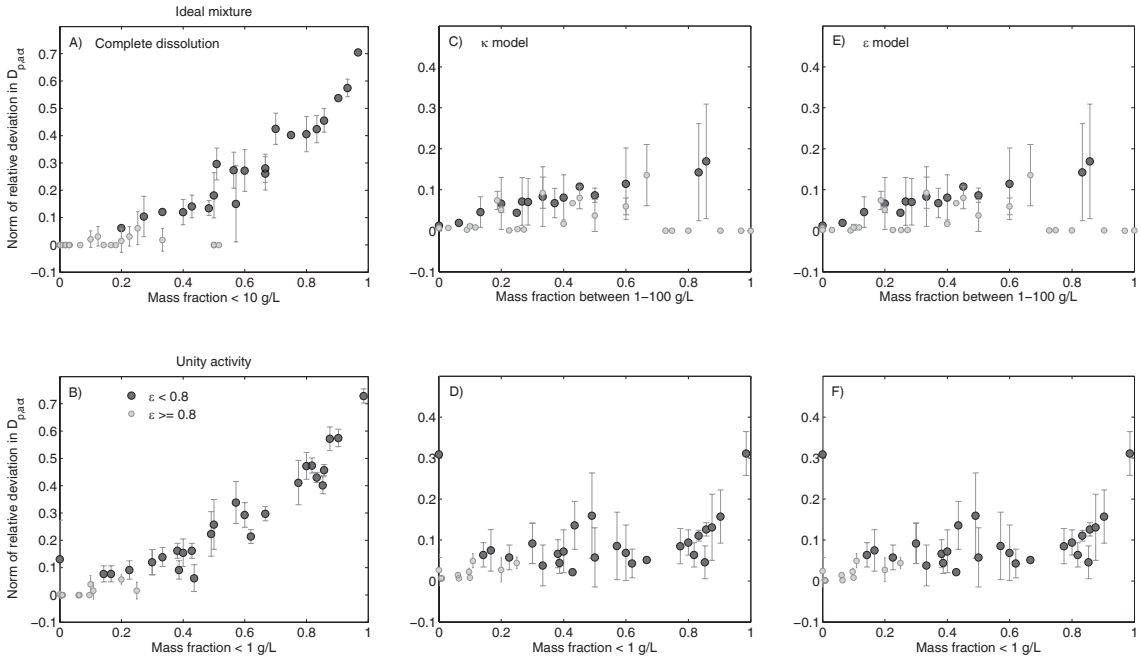

Figure 12. The solubility distribution properties best explaining the performance of the three simplified solubility models, illustrated with the norm of the relative deviation of $D_{\mathrm{p,act}}$ as compared with the full model predictions for $s = 1$, 0.6, 0.3 and 0.1 %. The performance of the complete dissolution assumption as a function of the mass fraction with solubilities below the median c_{t} for **(a)** the ideal organic mixture (median $c_{\mathrm{t}} = 10\,\mathrm{g\,L^{-1}}$) and **(b)** the unity organic activity (median $c_{\mathrm{t}} = 1\,\mathrm{g\,L^{-1}}$) assumptions. The performance of the κ model as a function of the mass fraction with solubilities **(c)** between 1 and $100\,\mathrm{g\,L^{-1}}$ for the ideal organic mixture assumption; and **(d)** below $1\,\mathrm{g\,L^{-1}}$ for the unity organic activity assumption. The performance of the ε model as a function of the mass fraction with solubilities **(e)** between 1 and $100\,\mathrm{g\,L^{-1}}$ for the ideal organic mixture assumption; and **(f)** below $1\,\mathrm{g\,L^{-1}}$ for the unity organic activity assumption. The points close to complete dissolution ($\varepsilon \geq 0.8$) are shown with lighter grey than the rest of the points. The error bars represent the variability with supersaturation and particle size.

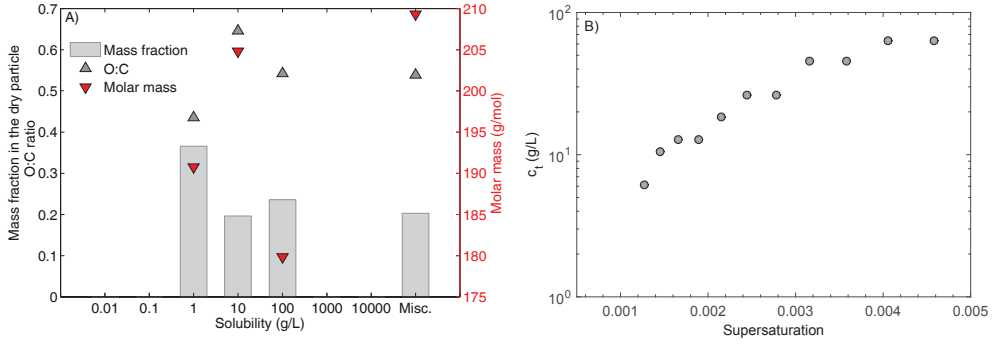

Figure 13. (a) An example of a solubility distribution for SOA generated in dark ozonolysis of α-pinene SOA. The expected composition has been taken from Chen et al. (2011), and the pure-component solubilities have been calculated with the SPARC prediction system (e.g., Wania et al., 2014, and references therein). "Misc." refers to completely miscible components. **(b)** The dependence of the c_{t} value at the point of activation on supersaturation assuming an ideal organic mixture, with only points corresponding to limited solubility ($0 < \varepsilon < 1$) displayed.

simplified descriptions of solubility: (1) assuming complete dissolution; (2) representing the mixture with single hygroscopicity parameter κ; and (3) representing the mixture with a single soluble fraction $\varepsilon_{\mathrm{eff}}$. The calculations were carried out for particle dry sizes ranging from 20 to 500 nm and supersaturations between 0.03 and 5 %, thus probing an atmospherically representative parameter space and resulting in a total of 5957 unique activation points.

Comparing the full model predictions to the simplified solubility descriptions, we find that assuming complete dissolution under-predicts the activation diameter up to a factor of about 2 for the studied mixtures. Our results indicate that

about 70–80 % of the material needs be dissolved at the point of activation for the complete dissolution assumption to predict activation diameters that are within 10 % of that produced by the full solubility treatment. Adding a single parameter to describe the mixture solubility improved the situation considerably: the predictions of activation diameters based on a single ε or κ for a given mixture were within 10 % of the full model predictions, the difference between these two approaches being only marginal.

The fitted soluble fractions, $\varepsilon_{\mathrm{eff}}$, describing the solubility distribution (and thus the fitted κ that is directly proportional to ε) were found to correspond well to the fraction of dry particle material with solubilities larger than a given threshold solubility c_{t}. For the ideal organic mixture assumption, the median c_{t} was $10\,\mathrm{g\,L^{-1}}$, most of the values falling between 1 and $100\,\mathrm{g\,L^{-1}}$, depending somewhat on the supersaturation. Since the material with solubilities outside this range can generally be treated as completely soluble or insoluble in CCN-activation calculations, the error made by using the single soluble fraction increased when a larger fraction of material was present in this critical range. For the unity activity case, the median c_{t} was $1\,\mathrm{g\,L^{-1}}$, but decreased with the number of components present in the mixture, n. For the range of $n = 3$–100 studied here, the typical c_{t} values were between 0.1 and $10\,\mathrm{g\,L^{-1}}$. Due to the asymmetric shape of the aqueous–organic-phase partitioning of the organics in the unity activity case, the simplified models performed better the more material with solubilities larger than c_{t} was present in the particles. In general, the median values for c_{t} represented the soluble fraction with a reasonable accuracy in most of the studied mixtures, although the exact composition of the mixtures varied considerably.

Our values for the limiting solubilities for complete dissolution are in agreement with the values of 3 and $1\,\mathrm{g\,L^{-1}}$ previously reported by Huff-Hartz et al. (2006) and Chan et al. (2008) based on experimental data on specific mixtures. Our results on the two different assumptions about the organic-phase activities indicate that the mixtures investigated by these past studies were probably somewhat non-ideal, where the compounds hindered each other's dissolution less than would be expected for a fully ideal mixture. On the other hand, in light of our findings, the observations of the close-to-complete dissolution of SOA at activation (Huff Hartz et al., 2005; Engelhart et al., 2008) indicate that the majority of the material in the studied SOA mixtures had solubilities larger than $10\,\mathrm{g\,L^{-1}}$. Our results suggest that even with vastly different solubility distributions one can yield very similar CCN-activation behavior (and consequently values of κ or ε), as the parameter that matters is the material above c_{t}.

The above results suggest that the solubility range corresponding to limited solubility in CCN activation is between 0.1 and $100\,\mathrm{g\,L^{-1}}$, and resolving the solubility distributions of aerosol mixtures outside this range provides little added value for understanding their CCN activation. In fact, this is probably a conservative estimate, as in most cases, most material below $1\,\mathrm{g\,L^{-1}}$ is practically insoluble and most material above $10\,\mathrm{g\,L^{-1}}$ completely soluble – even considering the uncertainty in the organic mixture activity. These results can be used to guide the representation of the cloud activation properties of complex mixtures, and provide quantitative support for the previous notion that knowing the water-soluble fraction of the aerosol mixture in question is the key in most applications. We provide quantitative estimates on how this soluble fraction should be defined in the case of complex mixtures, and when such a simplified model is not expected to perform well.

There are, however, some limitations to our approach to keep in mind when applying the results to laboratory experiments or atmospheric data. Since the focus of this work was strictly on the links between solubility and CCN activation, we did not explore in depth how variation of surface activity, molecular mass, pure-component density, the gas-droplet partitioning of the organic compounds or non-ideality of water with respect to the aqueous phase would affect the results (see also Suda et al., 2012, 2014; Topping et al., 2013). Furthermore, temperature was assumed to stay constant at 298 K. Since many of the thermodynamic properties relevant to CCN activation are temperature dependent (see, e.g., Christensen and Petters, 2012), future work investigating the impact of temperature on the phenomena studied here is needed. Furthermore, the solubility and organic-phase activity should naturally be linked to the aqueous-phase activity coefficients predicted and used in a number of previous studies (see, e.g., Topping et al., 2013, and references therein), although a lack of well-defined experimental data on organic-phase activities and mixture solubilities currently hinders quantitative evaluation of the current multiphase mixture thermodynamic models (see, e.g., Cappa et al., 2008). Evaluation of the concepts and approaches presented here (e.g., the solubility limits c_{t}) with laboratory studies on well-defined complex mixtures over a wide range of solubilities, supersaturations and particle diameters would therefore be warranted.

Another important future step would be applying the introduced solubility distribution framework in the atmospheric context. On the one hand, the framework is likely to be useful in modeling the evolution of the CCN activity of secondary organics. We expect the solubility distributions (and thus c_{t}) to depend on the SOA mixture properties such as the O : C ratio and the molar masses of the mixture constituents, which in turn evolve due to atmospheric chemistry (Kuwata et al., 2013; Suda et al., 2014), coupling the solubility distributions to the different dimensions of the VBS (Donahue et al., 2006, 2011, 2012; Kroll et al., 2011; Shiraiwa et al., 2014). A systematic study investigating the interlinkages between these variables in light of the available experimental data from field and laboratory would thus be a valuable future contribution. Furthermore, as atmospheric aerosol particles are typically mixtures of organic and inorganic constituents, the molecu-

lar interactions between atmospheric organics and inorganics as well as their effect on the pure-component solubility should be expanded. On the other hand, the solubility distribution can be used as a simplifying concept aiding in large-scale model simulations coupling atmospheric chemistry to the dynamics of cloud formation. With the assumptions applied here, the CCN-activation calculation itself is computationally relatively light, slowing down considerably only if n is on the order 10 000 or larger with typical present-day computational resources. Therefore, using the solubility distribution framework within an atmospheric model is a good option if accuracy beyond the simple one-parameter approaches is required, or as an intermediate tool linking atmospheric age to the effective ε or κ describing a given mixture.

Acknowledgements. Financial support from European Research Council project ATMOGAIN (grant 278277), Vetenskapsrådet (grant 2011-5120), and European Commission FP7 integrated project PEGASOS (grant 265148) is gratefully acknowledged.

Edited by: A. Nenes

References

Albrecht, B. A.: Aerosols, cloud microphysics, and fractional cloudiness, Science, 245, 1227–1230, 1989.

Asa-Awuku, A. and Nenes, A.: Effect of solute dissolution kinetics on cloud droplet formation: Extended Köhler theory, Geophys. Res., 112, D22201, doi:10.1029/2005JD006934, 2007.

Asa-Awuku, A., Engelhart, G. J., Lee, B. H., Pandis, S. N., and Nenes, A.: Relating CCN activity, volatility, and droplet growth kinetics of β-caryophyllene secondary organic aerosol, Atmos. Chem. Phys., 9, 795–812, doi:10.5194/acp-9-795-2009, 2009.

Asa-Awuku, A., Nenes, A., Gao, S., Flagan, R. C., and Seinfeld, J. H.: Water-soluble SOA from Alkene ozonolysis: composition and droplet activation kinetics inferences from analysis of CCN activity, Atmos. Chem. Phys., 10, 1585–1597, doi:10.5194/acp-10-1585-2010, 2010.

Banerjee, S.: Solubility of organic mixtures in water, Environ. Sci. Technol., 18, 587–591, 1984.

Cappa, C. D., Lovejoy, E. R., and Ravishankara, A. R.: Evidence for liquid-like and nonideal behavior of a mixture of organic aerosol components, P. Natl. Acad. Sci. USA, 105, 18687–18691, 2008.

Chan, M. N., Kreidenweis, S. M., and Chan, C. K.: Measurements of the hygroscopic and deliquescence properties of organic compounds of different solubilities in water and their relationship with cloud condensation nuclei activities, Environ. Sci. Technol., 42, 3602–3608, 2008.

Chen, Q., Liu, Y., Donahue, N. M., Shilling, J. E., and Martin, S. T.: Particle-phase chemistry of secondary organic material: Modeled compared to measured O : C and H : C elemental ratios provide constraints, Environ. Sci. Technol., 45, 4763, doi:10.1021/es104398s, 2011.

Christensen, S. I. and Petters, M. D.: The role of temperature in cloud droplet activation., J. Phys. Chem. A, 116, 9706–9717, doi:10.1021/jp3064454, 2012.

Cruz, C. N. and Pandis, S. N.: A study of the ability of pure secondary organic aerosol to act as cloud condensation nuclei, Atmos. Environ., 31, 2205–2214, doi:10.1016/S1352-2310(97)00054-X, 1997.

Cruz, C. N. and Pandis, S. N.: The effect of organic coatings on the cloud condensation nuclei activation of inorganic atmospheric aerosol, J. Geophys. Res., 103, 13111–13123, 1998.

Donahue, N. M., Robinson, A. L., Stanier, C. O., and Pandis, S. N.: Coupled partitioning, dilution, and chemical aging of semivolatile organics, Environ. Sci. Technol., 40, 2635–2643, 2006.

Donahue, N. M., Epstein, S. A., Pandis, S. N., and Robinson, A. L.: A two-dimensional volatility basis set: 1. organic-aerosol mixing thermodynamics, Atmos. Chem. Phys., 11, 3303–3318, doi:10.5194/acp-11-3303-2011, 2011.

Donahue, N. M., Kroll, J. H., Pandis, S. N., and Robinson, A. L.: A two-dimensional volatility basis set – Part 2: Diagnostics of organic-aerosol evolution, Atmos. Chem. Phys., 12, 615–634, doi:10.5194/acp-12-615-2012, 2012.

Duplissy, J., Gysel, M., Alfarra, M. R., Dommen, J., Metzger, A., Prevot, S. H., Weingartner, E., Laaksonen, A., Raatikainen, T., Good, N., Turner, S. F., McFiggans, G., and Baltensperger, U.: Cloud forming potential of secondary organic aerosol under near atmospheric conditions, Geophys. Res. Lett., 35, L03818, doi:10.1029/2007GL031075, 2008.

Duplissy, J., DeCarlo, P. F., Dommen, J., Alfarra, M. R., Metzger, A., Barmpadimos, I., Prevot, A. S. H., Weingartner, E., Tritscher, T., Gysel, M., Aiken, A. C., Jimenez, J. L., Canagaratna, M. R., Worsnop, D. R., Collins, D. R., Tomlinson, J., and Baltensperger, U.: Relating hygroscopicity and composition of organic aerosol particulate matter, Atmos. Chem. Phys., 11, 1155–1165, doi:10.5194/acp-11-1155-2011, 2011.

Dusek, U., Frank, G. P., Hildebrandt, L., Curtius, J., Schneider, J., Walter, S., Chand, D., Drewnick, F., Hings, S., Jung, D., Borrmann, S., and Andreae, M. O.: Size matters more than chemistry for cloud-nucleating ability of aerosol particles, Science, 312, 1375–1378, 2006.

Engelhart, G. J., Asa-Awuku, A., Nenes, A., and Pandis, S. N.: CCN activity and droplet growth kinetics of fresh and aged monoterpene secondary organic aerosol, Atmos. Chem. Phys., 8, 3937–3949, doi:10.5194/acp-8-3937-2008, 2008.

Engelhart, G. J., Moore, R. H., Nenes, A., and Pandis, S. N.: Cloud condensation nuclei activity of isoprene secondary organic aerosol, J. Geophys. Res., 116, D02207, doi:10.1029/2010JD014706, 2011.

Farmer, D. K., Cappa, C. D., and Kreidenmweis, S. M.: Atmospheric processes and their controlling influence on cloud condensation nuclei activity, Chem. Rev., 115, 4199–4217, doi:10.1021/cr5006292, 2015.

Goldstein, A. H. and Galbally, I. E.: Known and unexplored organic constituents in the earth's atmosphere, Environ. Sci. Technol., 41, 1514–1521, 2007.

Good, N., Topping, D. O., Duplissy, J., Gysel, M., Meyer, N. K., Metzger, A., Turner, S. F., Baltensperger, U., Ristovski, Z., Weingartner, E., Coe, H., and McFiggans, G.: Widening the gap between measurement and modelling of secondary organic aerosol properties?, Atmos. Chem. Phys., 10, 2577–2593, doi:10.5194/acp-10-2577-2010, 2010.

Hallquist, M., Wenger, J. C., Baltensperger, U., Rudich, Y., Simpson, D., Claeys, M., Dommen, J., Donahue, N. M., George, C., Goldstein, A. H., Hamilton, J. F., Herrmann, H., Hoffmann, T., Iinuma, Y., Jang, M., Jenkin, M. E., Jimenez, J. L., Kiendler-Scharr, A., Maenhaut, W., McFiggans, G., Mentel, Th. F., Monod, A., Prévôt, A. S. H., Seinfeld, J. H., Surratt, J. D., Szmigielski, R., and Wildt, J.: The formation, properties and impact of secondary organic aerosol: current and emerging issues, Atmos. Chem. Phys., 9, 5155–5236, doi:10.5194/acp-9-5155-2009, 2009.

Hori, M., Ohta, S., Murao, N., and Yamagata, S.: Activation capability of water soluble organic substances as CCN, Aerosol Sci., 34, 419–448, 2003.

Hoyle, C. R., Boy, M., Donahue, N. M., Fry, J. L., Glasius, M., Guenther, A., Hallar, A. G., Huff Hartz, K., Petters, M. D., Petäjä, T., Rosenoern, T., and Sullivan, A. P.: A review of the anthropogenic influence on biogenic secondary organic aerosol, Atmos. Chem. Phys., 11, 321–343, doi:10.5194/acp-11-321-2011, 2011.

Huff Hartz, K. E., Rosenoern, T., Ferchak, S. R., Raymond, T. M., Bilde, M., Donahue, N. M., and Pandis, S. N.: Cloud condensation nuclei activation of monoterpene and sesquiterpene secondary organic aerosol, J. Geophys. Res., 110, D14208, doi:10.1029/2004JD005754, 2005.

Huff-Hartz, K. E. H., Tischuk, J. E., Chan, M. N., Chan, C. K., Donahue, N. M., and Pandis, S. N.: Cloud condensation nuclei activation of limited solubility organic aerosol, Atmos. Environ., 40, 605–617, 2006.

Jimenez, J. L., Canagaratna, M. R., Donahue, N. M., Prevot, A. S. H., Zhang, Q., Kroll, J. H., DeCarlo, P. F., Allan, J. D., Coe, H., Ng, N. L., Aiken, A. C., Docherty, K. S., Ulbrich, I. M., Grieshop, A. P., Robinson, A. L., Duplissy, J., Smith, J. D., Wilson, K. R., Lanz, V. A., Hueglin, C., Sun, Y. L., Tian, J., Laaksonen, A., Raatikainen, T., Rautiainen, J., Vaattovaara, P., Ehn, M., Kulmala, M., Tomlinson, J. M., Collins, D. R., Cubison, M. J., Dunlea, E. J., Huffman, J. A., Onasch, T. B., Alfarra, M. R., Williams, P. I., Bower, K., Kondo, Y., Schneider, J., Drewnick, F., Borrmann, S., Weimer, S., Demerjian, K., Salcedo, D., Cottrell, L., Griffin, R., Takami, A., Miyoshi, T., Hatakeyama, S., Shimono, A., Sun, J. Y., Zhang, Y. M., Dzepina, K., Kimmel, J. R., Sueper, D., Jayne, J. T., Herndon, S. C., Trimborn, A. M., Williams, L. R., Wood, E. C., Middlebrook, A. M., Kolb, C. E., Baltensperger, U., and Worsnop, D. R.: Evolution of organic aerosols in the atmosphere, Science, 326, 1525–1529, doi:10.1126/science.1180353, 2009.

King, S. M., Rosenoern, T., Shilling, J. E., Chen, Q., and Martin, S. T.: Cloud condensation nucleus activity of secondary organic aerosol particles mixed with sulfate, Geophys. Res. Lett., 34, L24806, doi:10.1029/2007GL030390, 2007.

King, S. M., Rosenoern, T., Shilling, J. E., Chen, Q., and Martin, S. T.: Increased cloud activation potential of secondary organic aerosol for atmospheric mass loadings, Atmos. Chem. Phys., 9, 2959–2971, doi:10.5194/acp-9-2959-2009, 2009.

King, S. M., Rosenoern, T., Shilling, J. E., Chen, Q., Wang, Z., Biskos, G., McKinney, K. A., Pöschl, U., and Martin, S. T.: Cloud droplet activation of mixed organic-sulfate particles produced by the photooxidation of isoprene, Atmos. Chem. Phys., 10, 3953–3964, doi:10.5194/acp-10-3953-2010, 2010.

Kreidenweis, S. M., Petters, M. D., and DeMott, P. J.: Deliquescence-controlled activation of organic aerosols, Geophys. Res. Lett., 33, L06801, doi:10.1029/2005GL024863, 2006.

Kroll, J. H., Donahue, N. M., Jimenez, J. L., Kessler, S. H., Canagaratna, M. R., Wilson, K. R., Altieri, K. E., Mazzoleni, L. R., Wozniak, A. S., Bluhm, H., Mysak, E. R., Smith, J. D., Kolb, C. E., and Worsnop, D. R.: Carbon oxidation state as a metric for describing the chemistry of atmospheric organic aerosol, Nature Chem., 3, 133–139, 2011.

Kuwata, M., Shao, W., Lebouteiller, R., and Martin, S. T.: Classifying organic materials by oxygen-to-carbon elemental ratio to predict the activation regime of Cloud Condensation Nuclei (CCN), Atmos. Chem. Phys., 13, 5309–5324, doi:10.5194/acp-13-5309-2013, 2013.

Massoli, P., Lambe, A. T., Ahern, A. T., Williams, L. R., Ehn, M., Mikkil, A., J., Canagaratna, M. R., Brune, W. H., Onasch, T. B., Jayne, J. T., Petäjä, T., Kulmala, M., Laaksonen, A., Kolb, C. E., Davidovits, P., and Worsnop, D. R.: Relationship between aerosol oxidation level and hygroscopic properties of laboratory generated secondary organic aerosol (SOA) particles, Geophys. Res. Lett., 37, L24801, doi:10.1029/2010GL045258, 2010.

McFiggans, G., Artaxo, P., Baltensperger, U., Coe, H., Facchini, M. C., Feingold, G., Fuzzi, S., Gysel, M., Laaksonen, A., Lohmann, U., Mentel, T. F., Murphy, D. M., O'Dowd, C. D., Snider, J. R., and Weingartner, E.: The effect of physical and chemical aerosol properties on warm cloud droplet activation, Atmos. Chem. Phys., 6, 2593–2649, doi:10.5194/acp-6-2593-2006, 2006.

Petters, M. D. and Kreidenweis, S. M.: A single parameter representation of hygroscopic growth and cloud condensation nucleus activity, Atmos. Chem. Phys., 7, 1961–1971, doi:10.5194/acp-7-1961-2007, 2007.

Petters, M. D. and Kreidenweis, S. M.: A single parameter representation of hygroscopic growth and cloud condensation nucleus activity – Part 2: Including solubility, Atmos. Chem. Phys., 8, 6273–6279, doi:10.5194/acp-8-6273-2008, 2008.

Petters, M. D. and Kreidenweis, S. M.: A single parameter representation of hygroscopic growth and cloud condensation nucleus activity – Part 3: Including surfactant partitioning, Atmos. Chem. Phys., 13, 1081–1091, doi:10.5194/acp-13-1081-2013, 2013.

Petters, M. D., Wex, H., Carrico, C. M., Hallbauer, E., Massling, A., McMeeking, G. R., Poulain, L., Wu, Z., Kreidenweis, S. M., and Stratmann, F.: Towards closing the gap between hygroscopic growth and activation for secondary organic aerosol – Part 2: Theoretical approaches, Atmos. Chem. Phys., 9, 3999–4009, doi:10.5194/acp-9-3999-2009, 2009a.

Petters, M. D., Kreidenweis, S. M., Prenni, A. J., Sullivan, R. C., Carrico, C. M., Koehler, K. A., and Ziemann, P. J.: Role of molecular size in cloud droplet activation, J. Geophys. Res., 114, D07209, doi:10.1029/2008JD011532, 2009b.

Petters, M. D., Carrico, C. M., Kreidenweis, S. M., Prenni, A. J., DeMott, P. J., Collett Jr., J. L., and Hans Moosmüller, H.: Cloud condensation nucleation activity of biomass burning aerosol, J. Geophys. Res., 114, D22205, doi:10.1029/2009JD012353, 2009c.

Poulain, L., Wu, Z., Petters, M. D., Wex, H., Hallbauer, E., Wehner, B., Massling, A., Kreidenweis, S. M., and Stratmann, F.: Towards closing the gap between hygroscopic growth and CCN activation for secondary organic aerosols – Part 3: Influence of the chemical composition on the hygroscopic properties and

volatile fractions of aerosols, Atmos. Chem. Phys., 10, 3775–3785, doi:10.5194/acp-10-3775-2010, 2010.

Prausnitz, J. M., Lichtenhaler, R. M., and Gomez de Azevedo, E.: Molecular thermodynamics of fluid-phase equilibria, Prentice Hall PTR, Upper Saddle River, NJ, USA, 3 ed., 1998.

Prenni, A. J., Petters, M. D., Kreidenweis, S. M., DeMott, P. J. and Ziemann, P. J.: Cloud droplet activation of secondary organic aerosol, J. Geophys. Res., 112, D10223, doi:10.1029/2006JD007963, 2007.

Pruppacher, H. R. and Klett, J. D.: Microphysics of Clouds and Precipitation, 954 pp., Kluwer Acad., Norwell, Mass., 1997.

Psichoudaki, M. and Pandis, S. N.: Atmospheric aerosol water-soluble organic carbon measurement: a theoretical analysis, Environ. Sci. Technol., 47, 9791–9798, doi:10.1021/es402270y, 2013.

Rastak, N., Silvergren, S., Zieger, P., Wideqvist, U., Ström, J., Svenningsson, B., Maturilli, M., Tesche, M., Ekman, A. M. L., Tunved, P., and Riipinen, I.: Seasonal variation of aerosol water uptake and its impact on the direct radiative effect at Ny-Ålesund, Svalbard, Atmos. Chem. Phys., 14, 7445–7460, doi:10.5194/acp-14-7445-2014, 2014.

Raymond, T. M. and Pandis, S. N.: Cloud activation of single-component organic aerosol particles, J. Geophys. Res., 107, 4787, doi:10.1029/2002JD002159, 2002.

Raymond, T. M. and Pandis, S. N.: Formation of cloud droplets by multicomponent organic particles, J. Geophys. Res., 108, 4469, doi:10.1029/2003JD003503, 2003.

Rissler, J., Swietlicki, E., Zhou, J., Roberts, G., Andreae, M. O., Gatti, L. V., and Artaxo, P.: Physical properties of the sub-micrometer aerosol over the Amazon rain forest during the wet-to-dry season transition - comparison of modeled and measured CCN concentrations, Atmos. Chem. Phys., 4, 2119–2143, doi:10.5194/acp-4-2119-2004, 2004.

Seinfeld, J. H. and Pandis, S. N.: Atmospheric chemistry and physics: From air pollution to climate change, John Wiley, New York, 2006.

Shiraiwa, M., Berkemeier, T., Schilling-Fahnestock, K. A., Seinfeld, J. H., and Pöschl, U.: Molecular corridors and kinetic regimes in the multiphase chemical evolution of secondary organic aerosol, Atmos. Chem. Phys., 14, 8323–8341, doi:10.5194/acp-14-8323-2014, 2014.

Shulman, M. L., Jacobson, M. C., Charlson, R. J., Synovec, R. E., and Young, T. E.: Dissolution behavior and surface tension effects of organic compounds in nucleating cloud droplets, J. Geophys. Res., 23, 277–280, 1996.

Spracklen, D. V., Jimenez, J. L., Carslaw, K. S., Worsnop, D. R., Evans, M. J., Mann, G. W., Zhang, Q., Canagaratna, M. R., Allan, J., Coe, H., McFiggans, G., Rap, A., and Forster, P.: Aerosol mass spectrometer constraint on the global secondary organic aerosol budget, Atmos. Chem. Phys., 11, 12109–12136, doi:10.5194/acp-11-12109-2011, 2011.

Suda, S. R., Petters, M. D., Matsunaga, A., Sullivan, R. C., Ziemann, P. J., and Kreidenweis, S. M.: Hygroscopicity frequency distributions of secondary organic aerosols, J. Geophys. Res., 117, D04207, doi:10.1029/2011JD016823, 2012.

Suda, S. R., Petters, M. D., Yeh, K., Strollo, C., Matsunaga, A., Faulhaber, A., Ziemann, P. J., Prenni, A. J., Carrico, C. M., Sullivan, R. C., and Kreidenweis, S. M.: Influence of functional groups on organic aerosol cloud condensation nucleus activity, Environ. Sci. Technol., 48, 10182–10190, 2014.

Swietlicki, E., Hansson, H.-C., Hämeri, K., Svenningsson, B., Massling, A., Mcfiggans, G., Mcmurry, P. H., Petäjä, T., Tunved, P., Gysel, M., Topping, D., Weingartner, E., Baltensperger, U., Rissler, J., Wiedensohler, A., and Kulmala, M.: Hygroscopic properties of submicrometer atmospheric aerosol particles measured with H-TDMA instruments in various environments a review, Tellus B, 60B, 432–469, doi:10.1111/j.1600-0889.2008.00350.x, 2008.

Topping, D. O. and McFiggans, G.: Tight coupling of particle size, number and composition in atmospheric cloud droplet activation, Atmos. Chem. Phys., 12, 3253–3260, doi:10.5194/acp-12-3253-2012, 2012.

Topping, D. O., Barley, M., and McFiggans, G.: Including phase separation in a unified model to calculate partitioning of vapours to mixed inorganic–organic aerosol particles, Faraday Discuss., 165, 273–288, 2013.

Twomey, S.: Pollution and the planetary albedo, Atmos. Environ., 8, 1251–1256, 1974.

VanReken, T. M., Ng, N. L., Flagan, R. C., and Seinfeld, J. H.: Cloud condensation nucleus activation properties of biogenic secondary organic aerosol, J. Geophys. Res., 110, D07206, doi:10.1029/2004JD005465, 2005.

Varutbangkul, V., Brechtel, F. J., Bahreini, R., Ng, N. L., Keywood, M. D., Kroll, J. H., Flagan, R. C., Seinfeld, J. H., Lee, A., and Goldstein, A. H.: Hygroscopicity of secondary organic aerosols formed by oxidation of cycloalkenes, monoterpenes, sesquiterpenes, and related compounds, Atmos. Chem. Phys., 6, 2367–2388, doi:10.5194/acp-6-2367-2006, 2006.

Volkamer, R., Jimenez, J. L., San Martini, F., Dzepina, K., Zhang, Q., Salcedo, D., Molina, L. T., Worsnop, D. R., and Molina, M. J.: Secondary organic aerosol formation from anthropogenic air pollution: Rapid and higher than expected, Geophys. Res. Lett., 33, L17811, doi:10.1029/2006GL026899, 2006.

Wania, F., Lei, Y. D., Wang, C., Abbatt, J. P. D., and Goss, K.-U.: Novel methods for predicting gas-particle partitioning during the formation of secondary organic aerosol, Atmos. Chem. Phys., 14, 13189–13204, doi:10.5194/acp-14-13189-2014, 2014.

Wex, H., Hennig, T., Salma, I., Ocskay, R., Kiselev, A., Henning, S., Massling, A., Wiedensohler, A., and Stratmann, F.: Hygroscopic growth and measured and modelled critical super-saturations of an atmospheric HULIS sample, Geophys. Res. Lett., 34, L02818, doi:101029/2006GL028260, 2007.

Wex, H., Petters, M. D., Carrico, C. M., Hallbauer, E., Massling, A., McMeeking, G. R., Poulain, L., Wu, Z., Kreidenweis, S. M., and Stratmann, F.: Towards closing the gap between hygroscopic growth and activation for secondary organic aerosol: Part 1 – Evidence from measurements, Atmos. Chem. Phys., 9, 3987–3997, doi:10.5194/acp-9-3987-2009, 2009.

Zieger, P., Weingartner, E., Henzing, J., Moerman, M., de Leeuw, G., Mikkilä, J., Ehn, M., Petäjä, T., Clémer, K., van Roozendael, M., Yilmaz, S., Frieß, U., Irie, H., Wagner, T., Shaiganfar, R., Beirle, S., Apituley, A., Wilson, K., and Baltensperger, U.: Comparison of ambient aerosol extinction coefficients obtained from in-situ, MAX-DOAS and LIDAR measurements at Cabauw, Atmos. Chem. Phys., 11, 2603–2624, doi:10.5194/acp-11-2603-2011, 2011.